RSC Advances

PAPER

View Article Online
View Journal | View Issue

Cite this: *RSC Adv.*, 2014, **4**, 45679

The effect of K_2HPO_4 and $Al_2(SO_4)_3$ modified MCM-41 on the dehydration of methyl lactate to acrylic acid

Bin Wang,* Chao li, Qiangqiang Zhu and Tianwei Tan

Received 16th August 2014
Accepted 8th September 2014

DOI: 10.1039/c4ra08738k

www.rsc.org/advances

In this paper, $Al_2(SO_4)_3$ and K_2HPO_4 modified MCM-41 were developed as catalysts for efficient conversion of methyl lactate (ML) to acrylic acid (AA) and methyl acrylate (MA). By changing the loading amount of the two salts and their ratio, the catalytic performance was optimized and the highest AA + MA yield of 73.6% was achieved over the 45 wt% K_2HPO_4 and $Al_2(SO_4)_3$ (6 : 4)/MCM-41 catalyst at 410 °C. The physicochemical properties of the catalysts were investigated by various techniques including XRD, BET, NH_3-TPD, CO_2-TPD, pyridine adsorption-FTIR and CO_2 adsorption-FTIR. The 45% loading sample showed the smallest acidic amounts and a moderate basicity amount, and the acidic–basicity ratio was thought to be crucial for the AA selectivity. Further decrease or increase in the ratio would cause a drop in AA selectivity. Carbon deposition was the main reason for catalyst deactivation. The catalyst could be fully regenerated by air treatment and behaved with good activity after 10 regenerations.

1. Introduction

Acrylic acid is an extremely valuable chemical intermediate used to produce paint additives, adhesives, textile and leather treating agents and other products.[1–4] Oxidation of propene to acrylic acid is a commercial process[5] which is the major contributor for AA production. In recent years, the partial oxidation of propane to AA through a one-step process has drawn much attention.[5–8] However, all of the above routes are based on fossil resources. In recent years, the reduction of CO_2 emission has become a crucial problem in the chemical industry. Given the current robust forces driving sustainable chemical production and available biomass conversion technologies, biomass-based routes are expected to make a significant impact on the chemical industry for producing bulk chemicals in the future.[9–11] Methyl lactate and lactic acid are commodity chemicals produced from renewable biomass resources.[12–15] Dehydration of LA or ML to AA is an environmental protection rout, but there still remain some difficulties: besides the dehydration of LA or ML to achieve AA, some side reactions such as decarbonylation/decarboxylation, condensation, hydrogenation can also occur, which lead to low AA selectivity.[16] Moreover, compared with the dehydration reaction, decarbonylation/decarboxylation is a thermodynamic priority reaction. Therefore, the development of an efficient catalyst for dehydration is necessary and crucial for an eco-friendly and cost-effective process.

In the literature, several catalysts consisting chiefly of sulphates and phosphates of the group I and II metals, supported phosphates salts on NaY and calcium hydroxyapatites have been reported.[17–24] The catalytic dehydration rate of alcohol over catalyst is thought to be dependent on the catalyst surface properties. The dehydration of lactic acid over various metal sulphates was investigated by Tang. $BaSO_4$ was found to show an efficient activity with 99.8% lactic acid conversion and 74.0% acrylic acid selectivity.[25] The high activity was ascribed to the moderate acidity on its surface. This view was also supported by Huang.[26] The effect of rare earth metals (lanthanum, cerium, samarium, and europium) supported on NaY catalyst was investigated and decreased surface acidity density was considered to cause the activity improvement. As the importance of basicity property was noticed, the relationship between activity and acidic–basicity was established. S. Loridant prepared different alkaline earth phosphates by co-precipitation and gas phase dehydration of lactic acid was evaluated.[27] Correlation between acrylic selectivity of alkaline earth phosphates and the acid–base balance was clearly established. The AA selectivity was the highest for acid–base balance close to 1 and decreased significantly when this parameter increased. However, it was reported by Xu that for hydroxyapatites catalyst, the AA formation rate showed a volcano type dependence on this acidity–basicity ratio and the best ratio was 4 : 1, which was different from Loridant.[28] Quite recently, Jean-François Paul reported that lattice oxygen atoms could easily abstract a hydrogen atom from the methyl group of the lactic acid and this reaction led to carbanion formation with a lower activation energy than carbocation formation by direct C–OH breaking.[29] The simulation results indicated that the basicity sites may

Beijing Key Lab of Bioprocess, College of Life Science and Technology, Beijing University of Chemical Technology, Beijing 100029, China. E-mail: wangbin@mail.buct.edu.cn

facilitate a higher AA selectivity. In general, there is still some contradiction among all the conclusions and some new catalyst needs to be developed.

In this paper, K_2HPO_4 and $Al_2(SO_4)_3$ supported MCM-41 showed good AA selectivity and the reason was deduced from the acidic properties. In order to further investigate the relationship between structure and activity and to provide some guidance for catalyst design, some more catalysts with different loading amount and K_2HPO_4–$Al_2(SO_4)_3$ ratio were developed. The catalysts were further examined with XRD, FTIR, CO_2/NH_3-TPD and the relationship between acid–basic property and selectivity was discussed.

2. Experimental

2.1. Materials

ML (analytic grade) was obtained from Sinopharm Chemical Reagent Co. and deionized water was used for its dilution. The alkali phosphates and sulphates were obtained from Sigma-Aldrich. MCM-41 was purchased from the Nankai University (China).

2.2. Catalyst preparation

There were two steps for the two salts supported catalyst preparation. The first one was the impregnation with phosphate. 4 g of MCM-41 was added into 100 mL aqueous solution with a desired phosphate amount (1.2 g, 30 wt% of the support). The mixture was stirred at 80 °C for 3 h, and the resulting slurry was subjected to oven with air flow at 110 °C for 10 h, and the dried samples were then calcined at 550 °C for 3 h with a heating rate of 10 °C min^{-1}. In the second step, the obtained catalyst from step one was added into 100 mL aqueous solution with a desired sulphate amount (0.8 g 20 wt% of the support). The mixture was stirred at 80 °C for 3 h, and the resulting slurry was subjected to oven with air flow at 110 °C for 10 h. The dried samples were calcined at 550 °C with a heating rate of 10 °C min^{-1} and then pressed at 20 MPa for 10 min and crushed into particles of 20–40 mesh.

2.3. Catalyst evaluation

The evaluation of catalyst activity was carried out in an upright fixed-bed quartz reactor which was 8 mm in inner diameter and 300 mm in length. The reaction was operated at atmospheric pressure. A 2 g portion of catalyst was charged into the reactor, and the space above the catalyst bed was filled with quartz chips to ensure preheating of the in-coming ML-containing liquid. Before introduction of the feedstock, the sample was heated up in a flow of pure N_2 (30 mL min^{-1}) to a desired temperature at a rate of 10 °C min^{-1} and kept at this temperature for 0.5 h. Then a flow of LA liquid (1.2 mL h^{-1}) was introduced, and the products were collected at a cold trap. The analysis of the collected species was conducted using a gas chromatograph equipped with FID and HP-FFAP capillary column (0.32 mm 25 m), and lactic acid butyl ester was adopted as internal standard.

2.4. Catalysts characterization

Powder X-ray diffraction measurement was conducted on a Japan Science D/max-RB diffractometer employing Cu Kα radiation ($\lambda = 0.15418$ nm). The X-ray tube was operated at 45 kV and 150 mA. The specific surface areas and pore volumes of the catalysts were measured through nitrogen adsorption at 77 K using a Micrometrics ASAP 2020 instrument. Prior to adsorption, the samples were treated at 200 °C under vacuum for 3 h. The specific surface area was calculated according to the Brunauer–Emmett–Teller (BET) method.

The basic–acid properties of the samples were evaluated by the temperature-programmed desorption (TPD) of CO_2 and NH_3. The TPD profiles were normalized by sample weight. The sample (0.1 g) in a glass U-tube was preheated at 773 K for 1 h in He flow (20 mL min^{-1}), and then the catalyst was cooled from 773 K to room temperature. CO_2 or NH_3 (20 kPa) was introduced into the glass tube at room temperature for 30 min, and CO_2 or NH_3 was evacuated for 30 min at 373 K. The TPD measurements were conducted from 373 to 773 K at a heating rate of 10 K min^{-1}.

The FTIR spectra of pyridine (CO_2) adsorption were recorded in the range of 1000–4000 cm^{-1} on a Nicolet 6700 spectrometer. The samples were pressed into self-supporting wafers containing 20 mg of material, and then the wafers were mounted inside a Pyrex vacuum cell and degassed at 400 °C for 1 h. Samples were allowed to cool down to room temperature (RT), and pyridine vapor was admitted into the cell and adsorption lasted for 1 h.

3. Results

3.1. ML dehydration activity

The catalytic activities of the phosphate and sulphate modified MCM-41 catalysts in ML conversions were listed in Table 1. The conversions of ML by these catalysts over the controlled reaction conditions gave mainly AA, MA, acetaldehyde and other small amounts of gaseous by-products such as carbon monoxide and hydrogen. It could be seen that the modification with both K_2HPO_4 and $Al_2(SO_4)_3$ showed better AA selectivity compared with the single salt supported. Based on this, the effect of different K_2HPO_4 to $Al_2(SO_4)_3$ ratio on catalyst activity was to be investigated. The K_2HPO_4 to $Al_2(SO_4)_3$ ratio was chosen from 10 to 0 with the whole loading amount of 45 wt% and the results were shown in Fig. 1. Only the AA production was depicted since the amount of MA was too small compared with AA for each sample which were around 1–2%. For each ratio, the ML conversion was above 96% and there was a significant improvement in AA selectivity from the ratio 10 : 0 to 6 : 4. Further decrease of the K_2HPO_4–$Al_2(SO_4)_3$ ratio would result in a drop of AA selectivity. The selectivity to MA did not change remarkably within the whole range of the ratios. The highest AA selectivity could be obtained at the 6 : 4 ratio (K_2HPO_4–$Al_2(SO_4)_3$).

The effect of the two salts loading amount on catalyst activity was then investigated with the K_2HPO_4 to $Al_2(SO_4)_3$ ratio of 6 : 4 and the results were shown in Fig. 2. The ML conversion

Table 1 Catalytic activity of modified MCM-41 for dehydration of ML to AA and MA[a]

		Product selectivity		
Catalyst	ML conversion (%)	AA (%)	MA (%)	Acetaldehyde (%)
MCM-41	99	1	0.2	70
K_2HPO_4/MCM-41	93	43	2	45
K_2HPO_4 + $Al_2(SO_4)_3$/MCM-41	90	70	2	22
$Al_2(SO_4)_3$/MCM-41	95	0.8	0.1	72

[a] Conditions: calcination temperature 550 °C, reaction temperature 400 °C, catalyst: 2 mL, particle size: 20–40 meshes, carrier gas N_2: 30 mL min^{-1}, feed flow rate: 1.2 mL h^{-1} ML feedstock: 60 wt% in water.

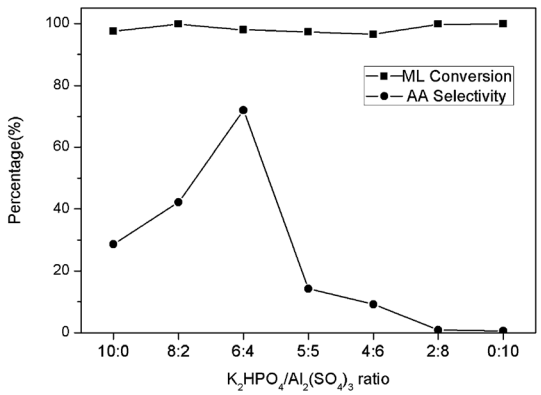

Fig. 1 ML dehydration activity of two salts modified MCM-41 with different ratio. Conditions: reaction temperature 410 °C, catalyst: 2 mL, particle size: 20–40 meshes, carrier gas N_2: 30 mL min^{-1}, feed flow rate: 1.2 mL h^{-1}, ML feedstock: 60 wt% in water. K_2HPO_4–$Al_2(SO_4)_3$/MCM-41 (45 wt%).

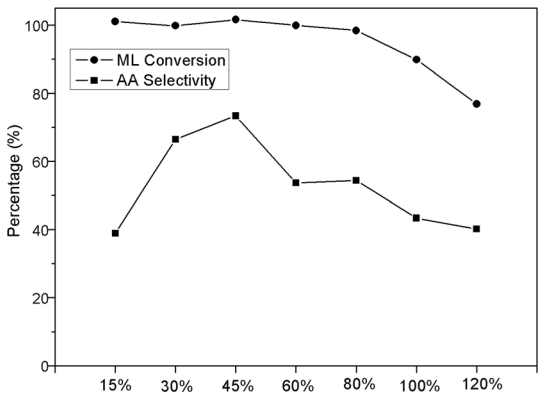

Fig. 2 ML dehydration activity of two salts modified MCM-41 with different loading amount. Conditions: reaction temperature 410 °C, catalyst: 2 mL, particle size: 20–40 meshes, carrier gas N_2: 30 mL min^{-1}, feed flow rate: 1.2 mL h^{-1}, ML feedstock: 60 wt% in water. K_2HPO_4–$Al_2(SO_4)_3$ = 6 : 4.

declined slowly as the loading amount increased in the range of 15–80 wt% and the conversions were all over 96%. When the loading amount was higher than 80%, there was a remarkable decrease of the conversion and the 120% loading sample showed the lowest conversion of 76%. A volcano type dependence appeared between the AA selectivity and the loading amount, and the highest AA selectivity was obtained at 45 wt% loading sample with the AA selectivity 72%. Further increase of the loading amount would result in a drop of AA selectivity.

3.2. Catalyst characterization

3.2.1. XRD. The X-ray diffraction (XRD) patterns of K_2HPO_4 and $Al_2(SO_4)_3$ modified MCM-41 catalysts were shown in Fig. 3 and 4 with different K_2HPO_4 and $Al_2(SO_4)_3$ ratios and different loading amounts respectively. MCM-41 only showed a wide diffraction peak around 22° ascribed to SiO_2 as shown in Fig. 3. After the impregnation of $Al_2(SO_4)_3$ or K_2HPO_4, some new peaks ascribed to $Al_2(SO_4)_3$ or $K_4P_2O_7$ appeared, which indicated that K_2HPO_4 condensed to $K_4P_2O_7$ after calcinations with no obvious change of $Al_2(SO_4)_3$. To the catalysts with two salts supported, $AlPO_4$ and K_2SO_4 generated, which should attribute to the reaction between phosphate and sulphate at high temperature. It could be seen that the peak intensity of K_2SO_4 varied as the K_2HPO_4–$Al_2(SO_4)_3$ ratio changed and the maximum appeared when K_2HPO_4–$Al_2(SO_4)_3$ ratio was 6 : 4. The increase in the peak intensity could be related to the amount of K_2SO_4 and the increase of crystallinity, which needed further explore.

As provided in Fig. 4, the effect of salts loading amounts on catalysts structure was investigated. As the loading amount

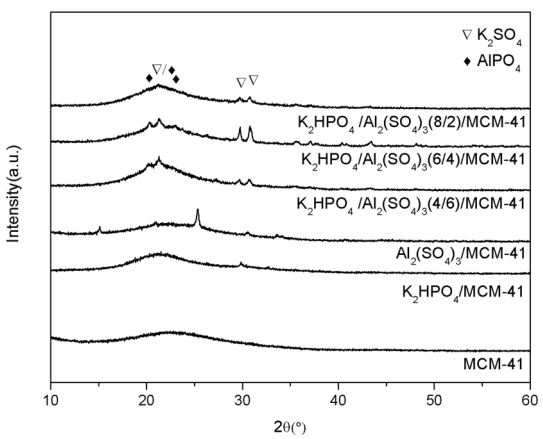

Fig. 3 XRD patterns of MCM-41 and modified catalysts with different K_2HPO_4–$Al_2(SO_4)_3$ ratio.

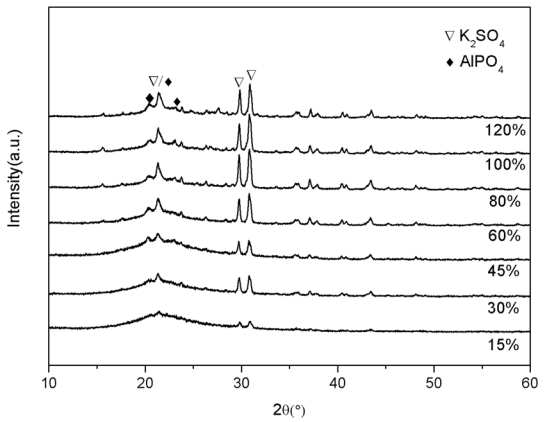

Fig. 4 XRD patterns of modified MCM-41 catalysts with different loading.

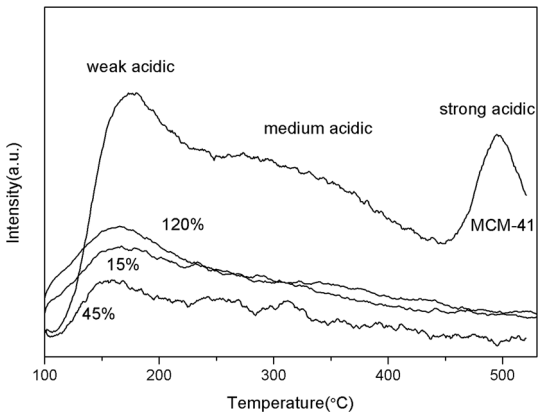

Fig. 5 NH_3-TPD profiles of MCM-41 and modified catalysts.

increased from 15% to 80%, the peak intensities of K_2SO_4 and $AlPO_4$ increased accordingly, indicating that more K_2SO_4 generated. However, there was no more increase when the loading amount was higher than 80%. Meanwhile, some more peaks such as the peaks centered at 18, 28° ascribed to some complex sulphate and phosphate appeared when the loading amount was higher than 45%. Combining the fact that the 45% loading sample showed the highest AA selectivity, it may indicate that the formation of complex sulphate and phosphate was detrimental for the selectivity. In other words, when the loading amount was 45%, the two precursors could completely react with each other and generate $AlPO_4$ and K_2SO_4.

The BET surface area and pore structure of all samples were shown in Table 2. MCM-41 sample showed the largest surface area of 1003 $m^2\ g^{-1}$ and the largest pore volume of 0.55 $cm^3\ g^{-1}$. The introduction of two salts with any amount would cause a decrease of surface area and pore volume. As the two salts loading amount increased from 15% to 120%, the BET surface area and pore volume decreased accordingly.

3.2.2. The acid–base properties. To estimate the surface acidity and basicity of the prepared catalysts, the TPD of CO_2 and NH_3 were carried out after N_2 pretreatments at 773 K. The intensity of each profile was normalized by the sample weight. Shown in Fig. 5 are the NH_3-TPD profiles recorded over the two salts modified MCM-41 with different loading amounts. The unmodified MCM-41 sample showed three desorption peaks centered at 177, 311, and 495 °C. With the two salts addition at elevated loading, the 311 °C desorption peak disappeared quickly; meanwhile, the peak at 495 °C also diminished. It was noted that the position of the weak acidic peaks shifted toward lower temperature. These observations suggested that the introduction of the two salts eliminated the sites of medium-strong acidity and reduced the density and strength of the sites of weak acidity. It also should be pointed out that compared with the other loading amounts, the supported catalyst with 45% loading amount showed the lowest acidic density. A higher or lower loading amount would lead to a larger acidic amounts.

Shown in Fig. 6 are the CO_2-TPD profiles recorded over the two salts modified MCM-41 with different loadings. The unmodified MCM-41 sample showed three desorption peaks centered at 485, 643, and 676 °C and the basic amount was 266 μmol g^{-1}. With the two salts addition at elevated loading, the 485 °C desorption peak diminished and only one peak in the range of 600–700 °C remained for all the modified samples. Based on the CO_2-TPD result, the 15% loading amount sample showed the largest basic amount of 441 μmol g^{-1}. There was a remarkable decrease of the basic density as the loading amount increased, and the 120% loading amount sample showed the smallest basic amount.

3.2.3. Pyridine adsorption FTIR. FTIR spectra of pyridine adsorption on parent and two salts modified MCM-41 were collected for the determination of Bronsted and Lewis acid sites, and the results were shown in Fig. 7. All the samples had bands around 1440 and 1600 cm^{-1}, attributable to pyridine adsorption on Lewis acid sites. The MCM-41 samples exhibited strong bands at 1450, 1490 and 1600, cm^{-1}. The 1490 cm^{-1} band can be ascribed to the Lewis and Bronsted acid sites.[30–33] It was noted that the characteristic band of pyridine adsorption on Bronsted acid sites at 1540 cm^{-1} was absent, so in the present case, the 1489 cm^{-1} band should be ascribed solely to

Table 2 Physicochemical properties of the modified catalysts with different loading amounts

Catalyst	S_{BET} ($m^2\ g^{-1}$)	Pore volume ($cm^3\ g^{-1}$)	Acid amount (μmol g^{-1})	Basic amount (μmol g^{-1})	*A*/*B*
0%	1003	0.55	720	266	2.7
15%	287	0.398	164	441	0.27
45%	48	0.29	86	45	1.91
120%	49	0.266	140	24	5.83

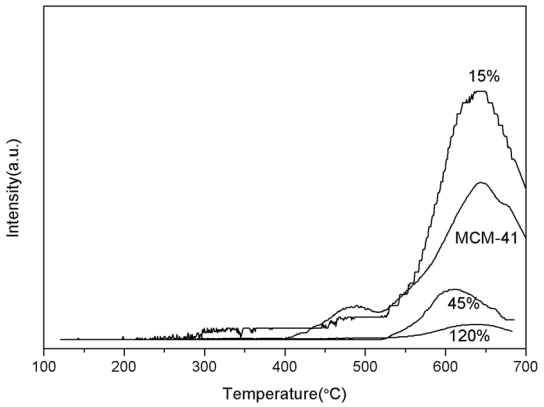

Fig. 6 CO_2-TPD profiles of MCM-41 and modified catalysts.

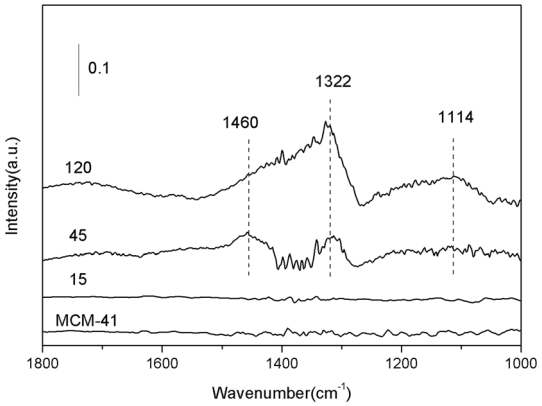

Fig. 8 FTIR spectra of CO_2 adsorption collected over unmodified and modified MCM-41.

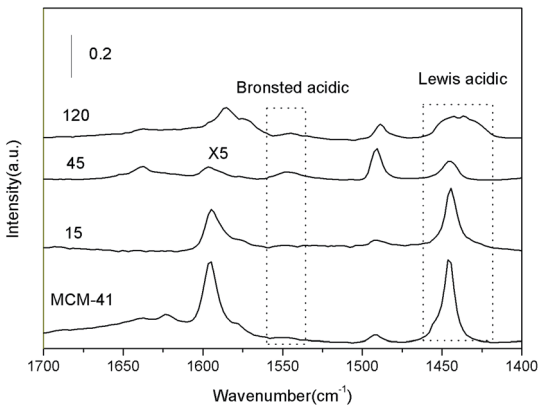

Fig. 7 FTIR spectra of pyridine adsorption collected over unmodified and modified MCM-41.

Lewis acid sites. This was a clear signal that the MCM-41 had mainly Lewis acid sites.

With the two salts supported together, the patterns varied with the loading amount. It could be seen that the 15% supported sample was similar to MCM-41. At higher loadings, the intensity of the 1440 cm^{-1} peak declined, suggesting that the Lewis acid sites associated with the framework of MCM-41 were blocked by the impregnation of two salts. To the 120% supported sample, it showed a broad peak around 1450 and 1600 cm^{-1}, indicating that some new Lewis acids associated with the two salts appeared besides the Lewis acid related to MCM-41. It should be pointed out that the bands intensities of 45% supported sample were really low compared with all the other samples, indicating that this sample had the smallest surface acid sites. This was consistent with the NH_3-TPD results.

3.2.4. CO_2 adsorption FTIR. Fig. 8 showed the infrared spectra of CO_2 adsorbed on the catalyst in the region 1800–1000 cm^{-1} for the four representative samples. It could be seen from the spectra that there was little surface basic sites on MCM-41 and 15% supported sample. Some basic sites (1460, 1322, 1114 cm^{-1}) which correspond to the monodentate and bulk-like carbonates adsorbed on the O^{2-} anions appeared when the loading amount increased, and the 120% sample showed the largest basic sites.[34] However, there is some contradiction between the CO_2-TPD and the IR results. Take the 15% sample as an example, according to the CO_2-TPD result in Fig. 6, it showed the largest basicity amount; but based on the CO_2-IR result it was nearly zero. One explanation of the contradiction could be that the IR result mainly reflected the surface information and the TPD result is thought to be the whole amount.

3.3. Catalytic activity optimization

3.3.1. Effect of reaction temperature. The conversion of ML could be critically influenced by reaction temperature and the effect of reaction temperature on catalyst performance was shown in Fig. 9. The reactions were carried out in the 320–450 °C range over the phosphate and sulphate modified catalyst with an optimized loading of 45 wt%. A notable increase in ML conversion was observed when the reaction temperature raised from 320 to 380 °C. Further increase of the temperature to 450 °C had little effect on ML conversion since the conversion was higher than 99% over 400 °C. The effect of reaction temperature on the AA selectivity was quite different from the

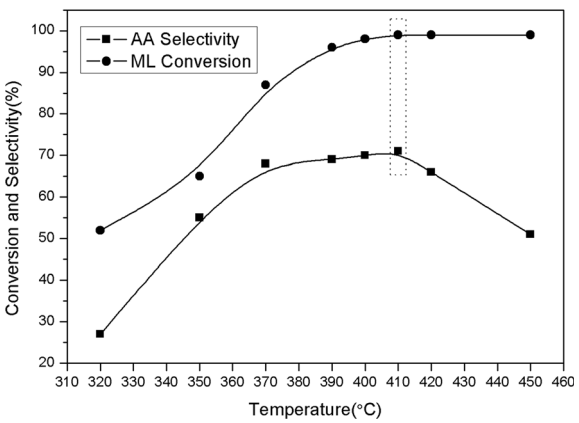

Fig. 9 ML conversion as well as AA selectivity. Conditions: catalyst: 2 mL, particle size: 20–40 meshes, carrier gas N_2: 30 mL min^{-1}, feed flow rate: 1.2 mL h^{-1}, ML feedstock: 60 wt% in water. K_2HPO_4–$Al_2(SO_4)_3$/MCM-41 (45 wt%).

ML conversion and there were three periods depending on the reaction temperature. Similar to the ML conversion profile, there was an obvious AA selectivity increase in the period of 320 to 370 °C. During the 380–410 °C, the AA selectivity almost remained unchanged and it reached a maximum at 410 °C with the AA selectivity of 72%. When the temperature was higher than 410 °C, there was a notable drop of AA selectivity. Why the AA selectivity behaved in this way should be explained from the point of the competition of the dehydration reaction with other side reactions. When the temperature was higher than 410 °C, more side reactions and further reaction of AA would be enhanced since at elevated temperature the stability of carboxyl group decreased, thus the AA selectivity decreased.

3.3.2. Effect of liquid hourly space velocity (LHSV). The influence of LHSV on reaction performance was shown in Table 3. The reactions were conducted at 410 °C with flow rate of ML changed from 0.4 to 5 mL h^{-1} (corresponding LHSV = 0.2–2.5 h^{-1}). Other operation conditions such as the flow rate of N_2 (30 mL min^{-1}) and concentration of LA (60 wt%) were retained. It was observed from Table 2 that ML conversion decreased from 98.0% to 59.9% as LHSV increased from 0.2 to 2.5 h^{-1}. At elevated LHSV, the contact time of ML with catalyst reduced, resulting in low ML conversion. However, AA selectivity increased from 59.2% to 71.0% as LHSV increased from 0.2 to 0.6 h^{-1}, and declined to 64.4% at LHSV of 2.5 h^{-1}. There was an optimal LHSV of 0.6 h^{-1} at which the highest AA yield of 72% could be achieved. The decrease in the AA selectivity at low LHSV may indicate the presence of diffusion limitations.

3.3.3. Effect of LA concentration. ML conversion and AA yield were affected not only by LHSV but also by ML concentration in solution. Therefore, the effect of ML concentration on reaction performance was also studied, and the results were depicted in Table 4. It could be seen that the ML conversions stayed 98.5% from 15 to 75 wt%; meanwhile, AA selectivity first gradually increased from 56.1% to 71.0% and then decreased to 68.3%. There was an optimal LA concentration in solution, namely, 60 wt%, at which the highest AA yield of 70.8% could be obtained.

3.3.4 .Catalyst stability. The stability of catalyst with time on stream was studied at 410 °C over the two salts supported MCM-41 with 45 wt% loading amount (LHSV = 0.6 h^{-1} and ML concentration = 60 wt%). In our stability test of 20 h period, the ML conversion decreased from 99% to 75%, but the AA selectivity remained unchanged except a drop from 71% to 63% in the first 5 hours. The reason for its deactivation may be attributed to the ML polymerization and carbon deposit on the catalyst since the color of the catalyst became black. Similar to SAPO-34 used in MTO reaction, our catalysts could also be regenerated by a simple treatment at 410 °C with air for 2 hours. The results could be seen in Fig. 10 that with a short treatment after 8 h test, the catalyst could be fully regenerated and the ML conversion and the AA selectivity mainly remained unchanged for 10 times reuse.

In order to investigate the reason for the catalyst deactivation, the fresh and used catalyst and the regenerated sample

Table 3 Reaction performance at various LHSV[a]

LHSV (h^{-1})	ML Conversion (%)	AA selectivity (%)	Acetaldehyde (%)	AA yield (%)
0.2	98.1	59.2	15.9	58.1
0.4	99.8	62.3	17.5	62.2
0.6	98.5	70.8	16.0	70.0
1	95.2	66.6	15.9	63.4
1.5	83.5	64.8	14.8	54.1
2.5	59.9	63.3	13.4	37.9

[a] Conditions: temperature: 410 °C, catalyst: 2 mL, particle size: 20–40 meshes, carrier gas N_2: 30 mL min^{-1}, ML feedstock: 60 wt% in water. K_2HPO_4–$AL_2(SO_4)_3$/MCM-41 (45 wt%).

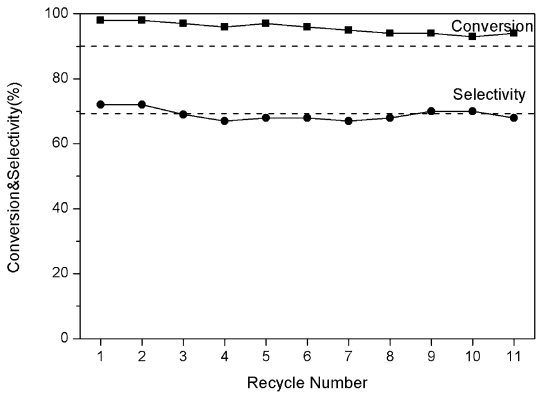

Fig. 10 Catalytic activity of the modified MCM-41 catalyst with 45% loading amount after 10 times regeneration for dehydration of ML to AA. Conditions: reaction temperature 410 °C, catalyst: 2 mL, particle size: 20–40 meshes, carrier gas N_2: 30 mL min^{-1}, feed flow rate: 1.2 mL h^{-1} ML feedstock: 60 wt% in water. K_2HPO_4–$Al_2(SO_4)_3$ = 6 : 4.

Table 4 Reaction performance at various ML concentrations in solution[a]

ML concentration (%)	ML conversion (%)	AA selectivity (%)	Acetaldehyde (%)	AA yield (%)
15	98.6	56.1	22	55.3
30	98.5	59.2	21	58.3
45	98.5	65.1	19	64.1
60	98.5	70.8	17	70.0
75	98.0	68.3	19	66.9

[a] Conditions: temperature: 410 °C, catalyst: 2 mL, particle size: 20–40 meshes, carrier gas N_2: 30 mL min^{-1}, feed flow rate: 1.2 mL h^{-1} K_2HPO_4–$AL_2(SO_4)_3$/MCM-41 (45 wt%).

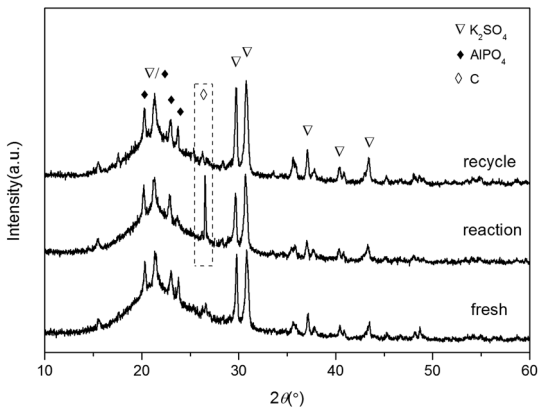

Fig. 11 XRD patterns of modified catalyst of fresh, reaction and recycle sample.

were examined with XRD (Fig. 11). It could be seen that the main peaks of the three samples were quite similar except the new peak centered at 26.6° belonging to graphite appeared for the reaction one. After the regeneration, the graphite peak disappeared and the profile became the same as the fresh one, indicating that the catalyst could be totally regenerated. Besides, it was proved that the dehydration reaction and the regeneration process had little effect on the catalyst structure, indicating that the samples could be promising industrial catalysts with its good stability.

4. Discussion

It has been known that the catalytic dehydration rate of alcohol over catalyst would be dependent on the catalyst surface acid–base property. An attempt is made to correlate the rates of ML conversion and AA formation with the surface acidity and basicity of the modified catalysts. The acidic amounts and basicity amounts calculated by $NH_3(CO_2)$-TPD as well as the ratio between acidic and basicity were shown in Table 1. MCM-41 showed the lowest AA selectivity due to its strong acidic sites. For the other three samples, the AA selectivity was negatively related to the acidic density and 45% sample showed the lowest acidic density and highest AA selectivity. Basic sites should play an important role in the dehydration reaction since it can dissociate H–C bond and enhance the dehydration reaction. In our study, the best AA selectivity appeared when the acid–basic = 1.91 on the 45% sample, which was different from the result of Xu (acidic–basicity = 4) and Loridant (acidic–basicity = 1). The difference may come from different catalysts and the precursors between LA and ML. In general, specific to this catalyst, the acid–basic ≈ 1.9 was best for the AA selectivity. The best acidic–basicity ratio varied on catalysts may attribute to the ML adsorption or consecutive reactions.

5. Conclusion

By modifying the loading amount and K_2HPO_4–$Al_2(SO_4)_3$ ratio, the surface acid–basic properties of MCM-41 based catalyst could be adjusted and used in ML dehydration reaction. 72% AA selectivity was achieved over 6 : 4 ratio of K_2HPO_4 and $Al_2(SO_4)_3$ and 45 wt% supported MCM-41 catalyst. The higher selectivity for acrylic acid should be correlated to the synergistic effect of the weaker acid site density and moderate basic site density as well as the acidic–basicity ratio. The catalyst showed a good stability and could be regenerated after air treatment.

Acknowledgements

The authors would like to acknowledge the Ministry of Science and Technology, PR China for the financial support of Project 2013CB733600. We would also thank China Postdoctoral Science Foundation (2013M530515).

References

1 L. F. Boesel and R. L. Reis, *Prog. Polym. Sci.*, 2008, **33**, 180–190.
2 C. M. Tang, Y. Zeng, X. G. Yang, Y. C. Lei and G. Y. Wang, *J. Mol. Catal. A: Chem.*, 2009, **314**, 15–20.
3 X. Xu, J. Lin and P. Cen, *Chin. J. Chem. Eng.*, 2006, **14**, 419–427.
4 V. Grabovac, D. Guggi and A. B. Schnürch, *Adv. Drug Delivery Rev.*, 2005, **57**, 1713–1723.
5 M. M. Lin, *Appl. Catal., A*, 2001, **207**, 1–16.
6 X. J. Yang, R. M. Feng, W. J. Ji and C. T. Au, *J. Catal.*, 2008, **253**, 57–65.
7 M. M. Lin, *Appl. Catal., A*, 2003, **250**, 305–318.
8 P. Botella, J. M. L. Nieto, B. Solsona, A. Mifsud and F. Márquez, *J. Catal.*, 2002, **209**, 445–455.
9 X. Tong, Y. Ma and Y. Li, *Appl. Catal., A*, 2010, **385**, 1–13.
10 P. Sun, D. H. Yu, Z. C. Tang, H. Li and H. Huang, *Ind. Eng. Chem. Res.*, 2010, **49**, 9082–9087.
11 P. Sun, D. H. Yu, K. M. Fu, M. Y. Gu, Y. Wang, H. Huang and H. H. Ying, *Catal. Commun.*, 2009, **10**, 1345–1349.
12 M. H. Gao, M. Hiratu, E. Toorisaka and T. Hano, *Bioresour. Technol.*, 2006, **97**, 2414–2420.
13 M. A. Abdel-Rahman, Y. Tashiro and K. Sonomoto, *Biotechnol. Adv.*, 2013, **31**, 877–902.
14 M. A. Abdel-Rahman, Y. Tashiro and K. Sonomoto, *J. Biotechnol.*, 2011, **156**, 286–301.
15 M. Jarvinen, L. Myllykoski, R. Keiski and J. Sohlo, *Bioseparation*, 2000, **9**, 163–166.
16 Y. Fan, C. Zhou and X. Zhu, *Catal. Rev.*, 2009, **51**, 293–324.
17 Y. Matsuura, A. Onda, S. Ogo and K. Yanagisawa, *Catal. Today*, 2014, **226**, 192–197.
18 Y. Matsuura, A. Onda and K. Yanagisawa, *Catal. Commun.*, 2014, **48**, 5–10.
19 C. M. Tang, J. S. Peng, G. C. Fan, X. L. Li, X. L. Pu and W. Bai, *Catal. Commun.*, 2014, **43**, 231–234.
20 J. Yan, D. H. Yu, P. Sun and H. Huang, *Chin. J. Catal.*, 2011, **32**, 405–411.
21 J. Yan, D. H. Yu, H. Li, P. Sun and H. Huang, *J. Rare Earths*, 2010, **28**, 803–806.
22 J. F. Zhang, Y. L. Zhao, M. Pan, X. Z. Feng, W. J. Ji and C. T. Au, *ACS Catal.*, 2011, **1**, 32–41.

23 V. C. Ghantani, S. T. Lomate, M. K. Dongare and S. B. Umbarkar, *Green Chem.*, 2013, **15**, 1211–1217.
24 J. F. Zhang, Y. L. Zhao, X. Z. Feng, M. Pan, J. Zhao, W. J. Ji and C. T. Au, *Catal. Sci. Technol.*, 2014, **4**, 1376–1385.
25 J. Peng, X. Li, C. Tang and W. Bai, *Green Chem.*, 2014, **16**, 108–111.
26 H. J. Wang, D. H. Yu, P. Sun, J. Yan, Y. Wang and H. Huang, *Catal. Commun.*, 2008, **9**, 1799–1803.
27 E. Blanco, P. Delichere, J. M. M. Millet and S. Loridant, *Catal. Today*, 2014, **226**, 185–191.
28 B. Yan, L. Z. Tao, Y. Liang and B. Q. Xu, *ACS Catal.*, 2014, **4**, 1931–1943.
29 C. Hammaecher and J. F. Paul, *J. Catal.*, 2013, **300**, 174–182.
30 B. Chakraborty and B. Viswanathan, *Catal. Today*, 1999, **49**, 253–260.
31 X. Shao, X. Zhang, W. Yu, Y. Wu, Y. Qin, Z. Sun and L. Song, *Appl. Surf. Sci.*, 2012, **263**, 1–7.
32 T. D. Conesa, J. M. Hidalgo, R. Luque, J. M. Campelo and A. A. Romero, *Appl. Catal., A*, 2006, **299**, 224–234.
33 C. Cai, H. Wang and J. Han, *Appl. Surf. Sci.*, 2011, **257**, 9802–9808.
34 F. Wang, N. Ta and W. J. Shen, *Appl. Catal., A*, 2014, **475**, 76–81.